High-Speed High-Precision Proximity Sensor for Detection of Tilt, Distance, and Contact

Keisuke Koyama , Makoto Shimojo, Taku Senoo , and Masatoshi Ishikawa

Abstract—We developed a fingertip-size proximity sensor that detects the distance to and the tilt angle of the surface of an object with the peak-to-peak distance error less than 1/129th (<31 μm) and the measuring time less than 1/10th (<1 ms) those of existing sensors. In addition, we realized the task of catching a fragile object (paper balloon) with a high-speed robot hand equipped with the sensor. High-speed, high-precision sensing enables contact detection independently of the contact force. We describe a robust contact detection method that does not depend on the reflectance, the tilt angle, or the shape of target objects surface. In experiments, we confirmed that the sensor could measure a distance of 2.85–20 mm (resolution: 44 μm in <3 mm) and a tilt angle of ±45° (error: 1.47°) for objects with reflectances of 18% and 90%. We demonstrated that the hand could catch the paper balloon when dropped from a height of about 20 cm without crushing it.

Index Terms—Perception for grasping and manipulation, sensor-based control, multifingered hands, proximity sensor.

I. INTRODUCTION

IN THIS letter, we describe a newly developed high-accuracy, high-speed proximity sensor for detecting the tilt of, distance and contact to an object. We also demonstrated high-speed catching of a fragile object (paper balloon) without crushing it by using a high-speed robot hand equipped with the sensor (Fig. 1(a)).

Conventionally, contact between a tactile sensor and an object is defined as the sensor output (contact force or pressure value) exceeding a threshold value. With this approach, however, in high-speed grasping, robot hands tend to break or damage fragile objects whose reaction force is extremely small.

In our approach on the other hand, we define contact as zero distance to the object. Distance-based control enables contact detection, allowing the robot hand to grasp a fragile object at high speed and with a soft touch.

Furthermore, after contact, force control is possible because the contact force can be estimated on the basis of accurate detection of the deformation of elastic parts on the sensor, as shown in Fig. 1(c). High-speed, high-accuracy measurement enables super tactile sensing which continuously detects the
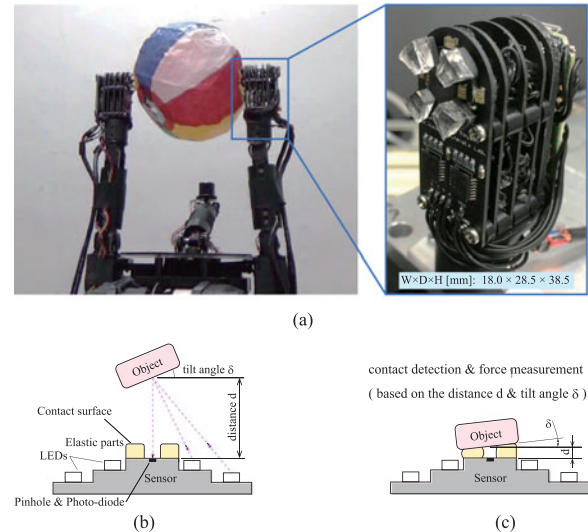
Fig. 1. (a) Overview of two fingers of the high-speed robot hand equipped with the proximity sensor. The sensor detects the distance to and the tilt angles of an object within 1ms with a resolution <50 μm. (b) In the non-contact state, the fingertip position and posture are adjusted by feedback of the distance d and the tilt angle δ. (c) In the contact state, contact detection and force measurement are also carried out by feeding back d and δ (deformation measurement of elastic body on the sensor). High-speed, high-accuracy measurement enables super tactile sensing which continuously detects the object from non-contact to contact state.

object from non-contact to contact state. The hand can grasp and manipulate the object reliably and at high speed.

We have developed a method of non-contact position control of fingers by mounting Resistor Network Structure Proximity Sensor on the fingertips of a robot hand [1]. We also developed an integrated control method for a multi-degree-of-freedom hand and arm using the sensor [2]. In our grasping strategy, first the approximate position of the object is detected by a vision sensor, and then the hand adjusts the grasping position and posture automatically by feedback from the proximity sensor and finally grasps the object. In previous research, we used such a proximity sensor only in a non-contact state. Currently, we plan to expand control of the robot hand by using proximity sensors not only in the non-contact state but also in the contact state. In this letter, as a first step to achieving this goal, we described the development of a high-accuracy, high-speed proximity sensor.

Several studies have addressed the challenge of detecting tactile information with a proximity sensor [3], [4]. Two types have been proposed: a capacitance type sensor having two detection

modes (tactile or proximity) [3] and an optical type sensor in which transparent rubber is arranged on the upper side of the sensor [4]. However, the optical and capacitance types are easily affected by the characteristics of the object (light reflectance, ambient environment, material, capacitance etc.), and it is not easy to achieve a resolution of 0.1 mm or less.

In addition, to detect the deformation of the fingertip surface and adjust the grasping force, it is necessary to measure the distance less than several millimeters and the tilt angles at a sampling time equivalent to the control period of the actuator (approximately 10 μs $\sim$ 1 ms). The measurement time of commercially available sensors is typically 7 to several tens of milliseconds, which is too long for high-speed control of the grasping force.

Therefore, we need to develop a fingertip-size proximity sensor that can detect the distance and the tilt angles with high accuracy and high speed.

A. Sensor Requirements

We developed a sensor that satisfies the following requirements.

- Minimum detection distance: <3 mm
- Maximum detection distance: 20 mm
- Distance resolution: <0.1 mm
- Detection range of the tilt angle: $\pm45°$
- Angle error:<1 ° (at the distance less than 3 mm)
- Measurement time: <1.0 ms
- Sensor dimensions W×D×H: 20 × 30 × 40 mm

The optical types [5]–[9] and capacitance types [10]–[14] are typically used in object grasping since these types can detect many kinds of objects. The sensor output of the capacitance type varies depending on the material, the volume, and the ground state of the object. A calibration method is necessary; however, a general method has not yet been realized. Methods that have been proposed for the optical type sensors, to compensate for the influence of the reflectance, include estimation of the tilt angle and distance while moving the sensor on the fingertip [5] and a calibration method using color information obtained by a vision sensor [6]. However, the distance accuracy is as large as several millimeters.

On the other hand, sequential manipulations have been realized by mounting optical time-of-flight (TOF) sensors on a gripper of a PR2 robot [7]. A low-cost ultra-tiny TOF sensor was also developed [8]. The optical TOF sensors can measure the distance independently of the reflectance since the distance value is calculated on the basis of the time until the reflected light reaches the detector. However, the resolution of these sensor is typically 1 mm, and the shortest measurement distance is approximately 10 mm. Therefore, the performance of these sensor is insufficient for detecting contact and measuring the deformation of the fingertip surface. With an optical TOF sensor, it is necessary to measure time with a precision of less than picosecond-order to realize a resolution of 1 mm or less. Although there is a method for decreasing the error by repeating measurements, this takes several milliseconds or more. Therefore, it is not easy to develop a proximity sensor that has a resolution of 1 mm and a measurement time of 1 ms or less.
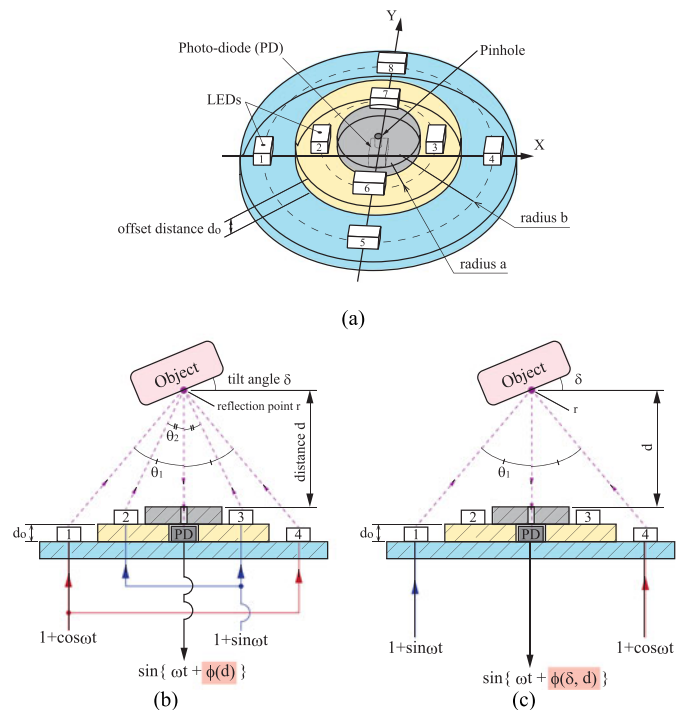

Fig. 2. (a) Arrangement of LEDs and detector (photo-diode) in the sensor. Eight LEDs are arranged around the photo-diode, and each LED is driven by two modulation signals. (b) In the distance mode, the distance d is detected from the phase $\phi(d)$ of the synthesized signal observed at the photo-diode. (c) In the tilt mode, the tilt angle δ is detected from the phase $\phi(\delta, d)$.

II. HIGH-SPEED HIGH-PRECISION PROXIMITY SENSOR

A. Principle and Design

We developed a proximity sensor that satisfies the above requirements on the basis of a principle proposed by Masuda *et al.* [15]. In the principle, LEDs emit light with two modulation signals, and the distance to and tilt angle of the object surface are measured from the phase of the combined wave observed at a detector (photo-transistor or photo-diode). Although this sensor uses reflected light intensity, it can measure the distance and tilt angle without being affected by the reflectance of the object surface by calculating the ratio of the received light intensities of the two modulated signals as the phase.

However, there were problems with the previous sensor [15], such as the large size (diameter: 80 mm), the slow response time (20 ms), and the low accuracy due to the large detection error ±2 mm.

In this letter, we introduce new optical designs allowing miniaturization of the sensor, and we also introduced a suitable high-accuracy analog circuit (two-phase lock-in amplifier). First, we explain the principle and optical design of the sensor, and then we describe the circuit.

Fig. 2(a) shows the positions of LEDs and the photo-diode. The photo-diode is arranged at the origin of the sensor XY plane, and eight LEDs are arranged at the intersection of circles of radii a and b centered on the origin and the X and Y axes. In the previous sensor [15], eight LEDs were arranged on the same plane. In our sensor, an offset distance d_o is newly set on the mounting surface of the inner and outer LEDs to adjust the

sensitivity of the sensor output. Also, a plate with a pinhole is placed in front of the photo-diode. These optical design features are for achieving high-precision measurement and miniaturizing the sensor.

The sensor has two modes: a distance mode and a tilt mode. In the distance mode, as shown in Fig. 2(b), LEDs 1 and 4 and LEDs 2 and 3 emit light with two modulated signals whose phase is shifted by 90 degrees. The distance is measured by detecting the phase $\phi(d)$ of the combined wave detected by the photo-diode. On the other hand, in the tilt mode, as shown in Fig. 2(c), LEDs 1 and 4 are used as modulated light sources. The tilt angle is measured from the phase $\phi(d, \delta)$ of the combined wave detected by the photo-diode. The following assumptions are made in the two modes.

1) The LEDs are point light sources and have no directivity.
2) The photo-diode has sharp directivity.
3) The emission frequency of LEDs is sufficiently faster than the moving frequency of a robot.
4) The object surface exhibits perfectly diffuse reflection.

Although specular reflection objects are excluded from the target objects due to assumption 4), assumptions 1) and 2) can be approximated well by selecting the LEDs and arranging the optical design. The emission frequency of the LEDs is set to several tens of kHz or more since the moving frequency of the robot is generally several tens to several hundred Hz.

B. Distance Mode

Here we describe the relationship between the phase $\phi(d)$ and the distance d to the object in the distance mode.

The photo-current flowing in the photo-diode is proportional to the irradiance of the object surface illuminated by the LEDs. The irradiance at the reflection point r is inversely proportional to the square of the optical path length since the LED is a point light source. Furthermore, the irradiance in the normal direction of the object surface is proportional to the cosine of the incident angle and the diffuse reflectance α since the surface exhibits diffuse reflection characteristics. Therefore, the photo-current flowing through the photo-diode is given by equation (1) (Details of the equation is described in [15]).

$$I_L = 2c\alpha \left(\frac{d I_0 (1 + \sin \omega t)}{(a^2 + d^2)^{3/2}} + \frac{(d + d_o) I_{90}(1 + \cos \omega t)}{(b^2 + (d + d_o)^2)^{3/2}} \right) \quad (1)$$

Here, c is the conversion factor from the irradiance to the photo-current, I_{0° and I_{90° are the radiation intensities of LEDs for the signal of phase $0°$ and the signal of phase $90°$, and ω is the emission frequency of the LEDs. a and b are the radii of the circles on which the inner and outer LEDs are arranged, d_o is the offset distance between the inner LEDs and outer LEDs, and d is the distance to the object surface.

According to assumption 3), the distance is almost same value in a short time Δt. The emission frequency of the LEDs, ω, dominates the time change of the photo-current. The time change of the photo-current is approximated by equation (2).

$$\frac{\Delta I_L}{\Delta t} \simeq 2c\alpha\omega \left(\frac{d I_0 \cos \omega t}{(a^2 + d^2)^{3/2}} - \frac{(d + d_o) I_{90} \sin \omega t}{(b^2 + (d + d_o)^2)^{3/2}} \right) \quad (2)$$
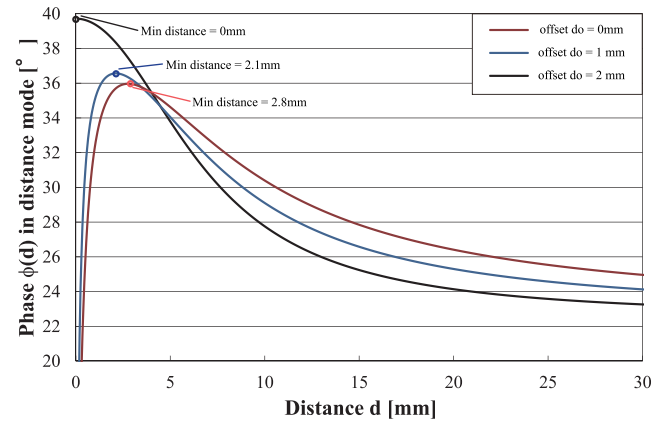

Fig. 3. Relation between offset distance d_o and phase $\phi(d)$ in the distance mode. Although the slope of the phase is increased by the offset distance d_o at a distance of 10 mm or more, the minimum detection distance becomes long. We adopted $d_o = 1$ mm (minimum detection distance of 2.1 mm) since we placed a 3 mm thick sheet of rubber on the pinhole plate.

We define the coefficient of $\cos \omega t$ as A, the coefficient of $\sin \omega t$ as B, $A/\sqrt{A^2 + B^2}$ as $\sin \phi(d)$, and $B/\sqrt{A^2 + B^2}$ as $\cos \phi(d)$. Equation (3) is obtained from additive theorem.

$$\frac{\Delta I_L}{\Delta t} \simeq A \cos \omega t - B \sin \omega t$$

$$\simeq \sqrt{A^2 + B^2} \left(\frac{A \cos \omega t}{\sqrt{A^2 + B^2}} - \frac{B \sin \omega t}{\sqrt{A^2 + B^2}} \right)$$

$$\simeq -\sqrt{A^2 + B^2} \sin(\omega t - \phi(d)) \quad (3)$$

Finally, the phase $\phi(d)$ in the distance mode is given by equation (4) (deriving from $\tan \phi(d) = A/B$).

$$\phi(d) = \tan^{-1} \left\{ \frac{I_0}{I_{90}} \frac{d}{d + d_o} \left(\frac{b^2 + (d + d_o)^2}{a^2 + d^2} \right)^{3/2} \right\} \quad (4)$$

The phase does not include the diffuse reflectance α of the object surface and the tilt angle δ. Therefore, the sensor can measure the distance independently of the reflectance and the tilt angle of the surface by detecting the phase $\phi(d)$.

Fig. 3 shows the phase when the offset distance d_o is 0 mm, 1 mm or 2 mm. Here, the emission intensities I_{0° and I_{90° are 1.0, and the arrangement intervals of the LEDs are $a = 4$ mm and $b = 7$ mm (actual size for mounting on the fingertip).

As shown in Fig. 3, the slope of the output at the distance of 15 mm or more is increased by the offset distance d_o. The output at longer distances is improved. However, the minimum detection distance increases to 0 mm, 2.1 mm, and 2.8 mm as d_o increases.

In order to realize deformation measurement of the rubber after contact, we adopted the offset distance $d_o = 1$ mm (minimum detection distance 2.1 mm) and placed a urethane rubber sheet with a thickness of 3 mm on the pinhole plate. The diameter of the pinhole was 1 mm, which is sufficiently smaller than 10 mm, since we assume that the sensor detects an object with a minimum width of 10 mm.
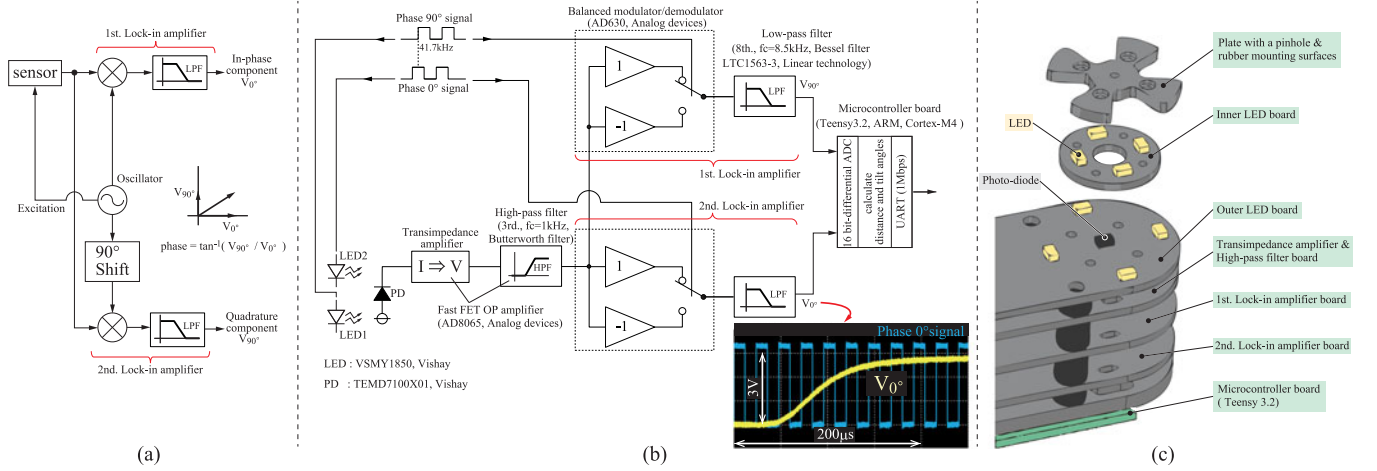
Fig. 4. (a) Block diagram of the 2-phase lock-in amplifier for measuring of the phase [16]. (b) Block diagram of the circuit of the proximity sensor. The phase of the signal is accurately detected by a two-phase lock-in amplifier. (c) Schematic diagram of the arrangement of the circuit board and the plate. We developed a fingertip-size module by dividing the processing circuits into six individual boards for each function and stacking the boards.

C. Tilt Mode

Here, we explain the relationship between the tilt angle δ of the object surface and the phase $\phi(\delta, d)$ of the signal.

In the tilt mode, LEDs 1 and 4 are used as the modulation light sources, and the photo-current I_L is given by equation (5) (Details of the equation is described in [15]).

$$I_L = \frac{c\alpha}{\cos\delta(b^2 + (d + d_o)^2)}(I_0(1 + \sin\omega t)\cos(\theta_1 - \delta)$$
$$+ I_{90}(1 + \cos\omega t)\cos(\theta_1 + \delta)) \tag{5}$$

Here, δ is the tilt angle of the surface, and θ_1 is the light incident angles of the outer LEDs with respect to the surface. The time change of photo-current is given by equation (6).

$$\frac{\Delta I_L}{\Delta t} \simeq \frac{c\alpha\omega}{\cos\delta(b^2 + (d + d_o)^2)}(I_0\cos\omega t\cos(\theta_1 - \delta)$$
$$- I_{90}\sin\omega t\cos(\theta_1 + \delta))$$

$$\frac{\Delta I_L}{\Delta t} \simeq A'\cos\omega t - B'\sin\omega t$$

$$\simeq \sqrt{A'^2 + B'^2}\left(\frac{A'\cos\omega t}{\sqrt{A'^2 + B'^2}} - \frac{B'\sin\omega t}{\sqrt{A'^2 + B'^2}}\right)$$

$$\simeq -\sqrt{A'^2 + B'^2}\sin(\omega t - \phi(\delta, d)) \tag{6}$$

Here, A' is the coefficient of $\cos\omega t$ and B' is the coefficient of $\sin\omega t$ in the tilt mode. Therefore the phase $\phi(\delta, d)$ in the tilt mode is given by equation (7).

$$\phi(\delta, d) = \tan^{-1}\left(\frac{I_0}{I_{90}}\frac{d + d_o + b \cdot \tan\delta}{d + d_o - b \cdot \tan\delta}\right) \tag{7}$$

The phase $\phi(\delta, d)$ does not include the reflectance α of the object surface. The sensor can measure the tilt angle that does not depend on the reflectance. When calculating the tilt angle δ, we calibrate the phase value $\phi(\delta, d)$ on the basis of the distance value detected in the distance mode since the phase $\phi(\delta, d)$ includes the distance.

D. Circuit

Masuda *et al.* [15] developed a sensor module with a band-pass filter and logic circuits. However, high-accuracy and small-size sensor was not realized because the band-pass filter has a disadvantage that the center frequency changes depending on the temperature characteristics of resistors and capacitors of the filter. And it is difficult to design a compact band-pass filter with a high quality factor.

We realized high-precision measurement and compact-size circuit by introducing a two-phase lock-in amplifier circuit. Fig. 4(a) shows the block diagram of the circuit and the phase of sensor signal is given by equation [17].

$$\phi = \tan^{-1}(V_{90°}/V_{0°}) \tag{8}$$

$V_{0°}$ is the voltage output of the first lock-in amplifier which is operated based on the phase 0 degree signal. On the other hand, $V_{90°}$ is the voltage output of the second lock-in amplifier which is operated based on the phase 90 degree signal.

In this letter, we used following equations instead of equation (8) to minimize the calculation time of the phase in a microcontroller.

$$V_{rate-d} = V_{90°}/V_{0°} \qquad \text{(indistancemode)} \tag{9}$$

$$V_{rate-\delta} = \frac{V_{90°}/V_{0°} - 1}{V_{90°}/V_{0°} + 1} \quad \text{(in tilt mode)} \tag{10}$$

V_{rate-d} and $V_{rate-\delta}$ are normalized voltage output in the distance mode and the tilt mode.

The circuit is suitable for high-precision measurement since the lock-in amplifier ideally has an infinite quality factor. And the output is not affected by the error of cut-off frequency of the high-pass and low-pass filter. The circuit can be miniaturized by using AD630 (Balanced modulator/demodulator, Analog Devices) and LTC1563-3 (Low-pass filter, Linear Technology).

Fig. 4(b) shows the block diagram of our proximity sensor. The photo-current is amplified by a transimpedance amplifier and is passed through a wideband high-pass filter (3rd order,

$f_c = 1$ kHz, Butterworth filter) to extract the AC voltage. The AC voltage is demodulated by AD630 on the basis of the modulation signals of the LEDs and is smoothed by the Low-pass filter (8th order, $f_c = 8.5$ kHz, Bessel filter). Finally, the two voltage signals are AD converted by Teensy 3.2 (Microcontroller board, ARM, Cortex-M4), and the phase is calculated.

The offset voltage due to ambient light and the detector is cut by the high-pass filter. In addition, the phase-shifted noise from the modulation signals is removed by the lock-in amplifier. Therefore, the circuit has extremely low noise.

In order to realize the measurement time of 1 ms, the cutoff frequency of the low-pass filter was set so that the settling time of the circuit was 200 μs. The distance measurement was completed in 256 μs since the time required for one AD conversion was 56 μs. When detecting the distance and two tilt angles, the measurement time was 768 μs.

In order to miniaturize the circuit, rectangular waves were used as the modulation signals of the LEDs. When rectangular waves are used, the odd-order component of the frequency is demodulated as noise. Therefore, the frequency of the modulation signal was set to 41.67 kHz, which was different from the control frequencies of the actuators and the commercial power supply.

We developed a fingertip-size module by dividing these processing circuits into six individual functions implemented on separate boards and stacking the boards (Fig. 4(c)).

III. EVALUATION OF THE SENSOR

We evaluated the detection range, the accuracy and the resolution of the distance and tilt angle.

The voltage values were measured by an AD converter of Teensy 3.2. The distance and tilt angle were calculated and transmitted to a PC via UART. In order to reduce the noise of the AD converter, outlier values were removed by a median filter (window size of 5) in Teensy 3.2. One AD conversion time was 56 μs (synchronized read of 2 ch in one shot mode, 16 bit differential, ADC clock frequency = 6.2 MHz, hardware averaging = 8, sampling speed = 0.97 μs), and the update rate of the median filter was 1 sample every 1 ms. These times had little influence on the total measurement time.

In the experiments, the distance and tilt angle between the sensor and the object were changed using an automatic rotation stage (OSMS-60YAW, SIGMAKOKI) and an automatic X stage (OSMS20-85, SIGMAKOKI) for high-precision experiments. The repeated positioning accuracy of the rotation stage was $0.02°$, and that of the X stage was 3 μm. We defined the distance d as the moving distance of the X stage and the tilt angle δ as the rotation angle of θ stage, since the repeated positioning accuracy is sufficiently high.

A. Distance Detection

Fig. 5(a) and (b) shows the sensor output in the distance mode for Kodak Gray Cards 90% and 18%.

In Fig. 5(a), the horizontal axis is the distance d to the object surface, and the vertical axis is the voltage ratio V_{rate-d}. In (b), the horizontal axis is the tilt angle δ of the object surface, and the
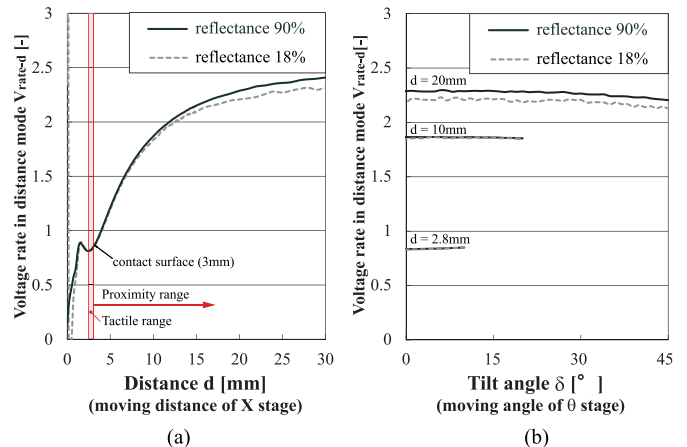

Fig. 5. Sensor output in distance mode. (a) Distance d vs. voltage ratio V_{rate-d} at tilt angle $\delta = 0$. (b) Tilt angle δ vs. voltage ratio V_{rate-d} at various fixed distances. The output V_{rate-d} did not depend on the reflectance and the tilt angle of the object surface.

vertical axis is the voltage ratio V_{rate-d}. Each line in the graph shows the result at a fixed distance.

As shown in Fig. 5(a), the voltage ratio V_{rate-d} monotonically increased from the distance of 2.7 mm, and the outputs in each object were almost on the same curve at short distances. Thus, the sensor could measure the distance accurately for the case of short distances. Although the minimum detection distance was 2.7 mm, since we placed a urethane rubber sheet with a thickness of 3 mm on the pinhole plate, the deformation of the rubber of up to 0.3 mm after contact could be measured.

As shown in Fig. 5(b), the voltage ratio V_{rate-d} kept almost a constant value, even when the tilt angle δ changed. Therefore, the sensor could accurately measure the distance in the vertical direction of the sensor surface.

Next, in order to evaluate the accuracy and the resolution of the distance detection, we converted the distance output d_{out} [mm] from V_{rate-d} [-] using a lookup table and a linear interpolation (equation (11)).

$$d_{out} = a_{d(i)} V_{rate-d} + b_{d(i)} \qquad (11)$$

Here, $a_{d(i)}$ is the slope of the linear interpolation in the table and $b_{d(i)}$ is also the intercept. i is the index number of the table. The voltage ratio, slope $a_{d(i)}$ and intercept $b_{d(i)}$ for each 0.1 mm section were calculated from experimental data (Fig. 5(a), reflectance 90%) and the table was created. In the distance conversion, a section including the measured voltage ratio was searched, and the distance was calculated by equation (11).

Fig. 6 (box-whisker plot) shows the results obtained when measuring the distance 10 times at each distance. We used a Kodak Gray Card 90% and 18% as the target object and measured the distance every 50 μm in the range 2.75 $\sim$ 3 mm. The horizontal axis is the distance to the object d, and the vertical axis is the distance output d_{out}. STD under the error bar is the standard deviation, and MEAN is the average value of the 10 measurement results.
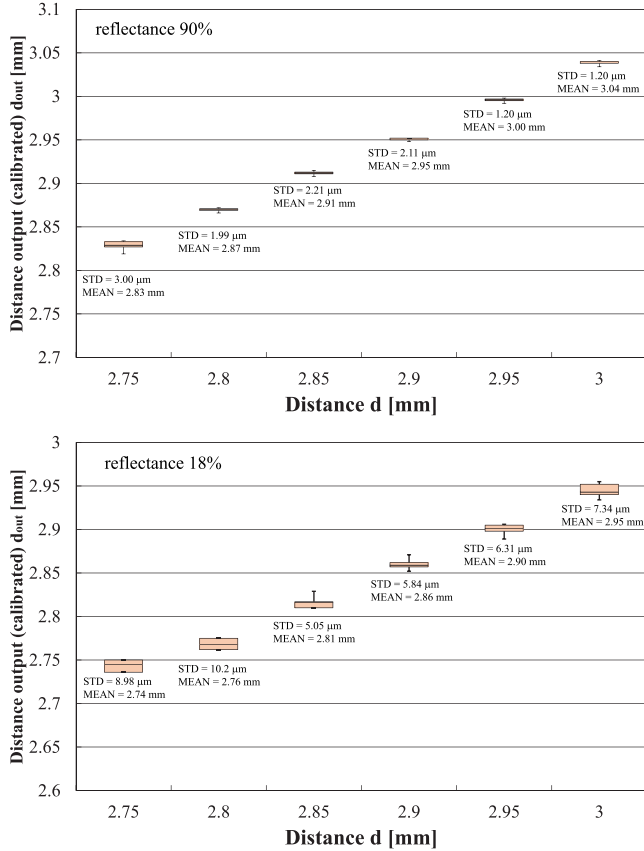
Fig. 6. Boxplots of 10 measurement results of the distance in the range of 2.75 to 3.0 mm for Kodak Gray Card 90% and 18%. If one resolution step is regarded as six-times of the maximum STD($\pm 3\max(\sigma)$), the distance resolution is 44 μm in the range of 2.85 to 3.0 mm.

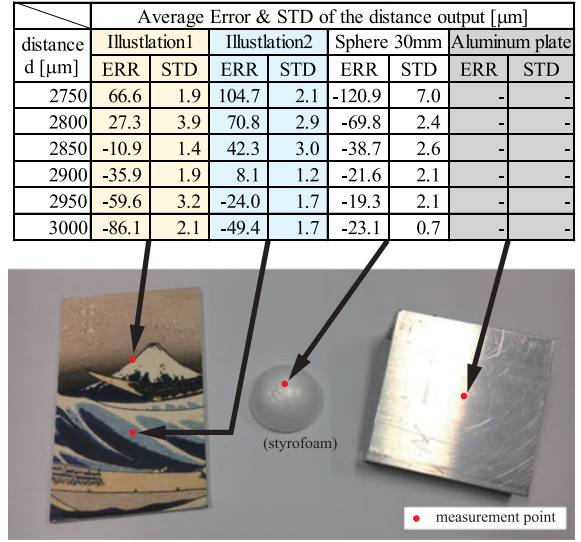| distance d [μm] | Average Error & STD of the distance output [μm] | | | | | | | |
| | Illustlation1 | | Illustlation2 | | Sphere 30mm | | Aluminum plate | |
	ERR	STD	ERR	STD	ERR	STD	ERR	STD
2750	66.6	1.9	104.7	2.1	-120.9	7.0	-	-
2800	27.3	3.9	70.8	2.9	-69.8	2.4	-	-
2850	-10.9	1.4	42.3	3.0	-38.7	2.6	-	-
2900	-35.9	1.9	8.1	1.2	-21.6	2.1	-	-
2950	-59.6	3.2	-24.0	1.7	-19.3	2.1	-	-
3000	-86.1	2.1	-49.4	1.7	-23.1	0.7	-	-

Fig. 7. Average error of the detected distance in 10 measurement results, and the standard deviation. ERR = (Average of 10 measurements) - distance d, STD = Standard Deviation of 10 measurements.
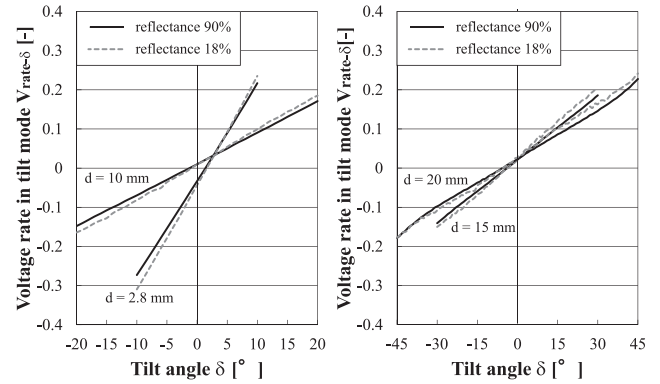

Fig. 8. Sensor output in tilt mode. The output $V_{\text{rate}-\delta}$ was almost proportional to the tilt angle δ, independently of the reflectance of the object.

As shown in Fig. 6, the variation of the detected distance is very small. If one resolution step is regarded as six-times the maximum STD ($\pm 3\max(\sigma)$), the distance resolution is 13.3 μm in the range of 2.85 to 3.0 mm for reflectance 90%. And the average error is 60 μm at the maximum. On the other hand for reflectance 18%, the distance resolution is 44.2 μm and average error is 50 μm at the maximum.

Peak-to-peak distance error is 31.0 μm at the maximum. On the other hand, the peak-to-peak error of a commercially available TOF sensor is 4 mm(± 2 mm) [7]. The peak-to-peak error of our sensor is less than 1/129-th of a commercially available sensor.

Fig. 7 shows the average error and the standard deviation of the distance output d_{out} for an illustrated paper, a styrofoam sphere ($d = 30$ mm) and an aluminum plate. In the figure, Err is the subtraction value of average of 10 measurement results and the distance d. STD is standard deviation of 10 measurement results.

From the results of the illustrations 1 and 2 in Fig. 7, when the color of the surface is not uniform, the error of the distance measurement tends to increase. The maximum error is -86.1 μm and the distance resolution is 19.2 μm ($\pm 3\max(\sigma)$) in the range of 2.85 to 3.0 mm. From the result of the sphere, the maximum error is -38.7 μm and the resolution is 15.6 μm ($\pm 3\max(\sigma)$) in the range of 2.85 to 3.0 mm. The sensor can measure the distance precisely for illustrations and the styrofoam sphere.

However, the sensor could not detect the aluminum plate. Since we assumes the detected object as a diffuse reflection characteristic, the sensor is difficult to measure the distance to the specular reflection surface.

Wang *et al.* [18] realized distance detection both of diffuse and specular reflection surface by measuring the rate of change of reflected light intensity during the sensor vibration. We infer that detection of the specular reflection surface can be realized by introducing this method.

B. Tilt Angle Detection

Fig. 8 shows the tilt detection characteristic of the sensor output in the tilt mode for Kodak Gray Cards 90% and 18%.

The horizontal axis is the tilt angle δ, and the vertical axis is the voltage ratio $V_{\text{rate}-\delta}$. Each line in the graph shows the results at a fixed distance.

From the figure, the voltage ratio $V_{\text{rate}-\delta}$ was almost proportional to the tilt angle δ, independently of the reflectance of the object. The voltage ratio $V_{\text{rate}-\delta}$ varied with almost constant slope and intercept for each distance.
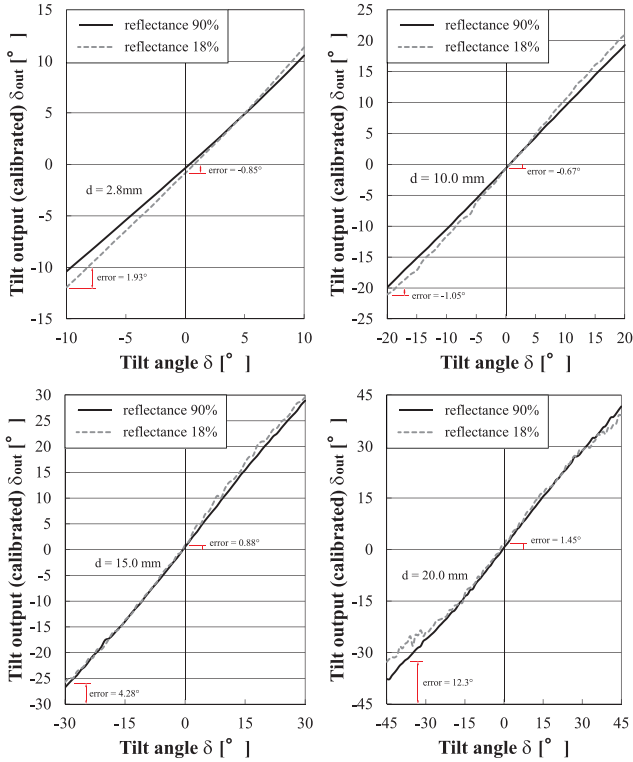
Fig. 9. Actual tilt angle detected by the sensor. The error at the origin was kept small by calibration. At a distance of 2.8 mm, the error was $-0.85°$.

In order to evaluate the error of the tilt detection, we converted the tilt output [°] from $V_{\text{rate}-\delta}$ [-] using a lookup table and a linear interpolation. We calculated the slope and intercept for every fixed distance and created the lookup table from the experimental data (Fig. 8, reflectance 90%) and converted the tilt output from $V_{\text{rate}-\delta}$ using following equations.

$$a'_\delta = a_{\delta(j)} + (a_{\delta(j+1)} - a_{\delta(j)})\frac{d_{\text{out}} - d_{(j)}}{d_{(j+1)} - d_{(j)}} \quad (12)$$

$$b'_\delta = b_{\delta(j)} + (b_{\delta(j+1)} - b_{\delta(j)})\frac{d_{\text{out}} - d_{(j)}}{d_{(j+1)} - d_{(j)}} \quad (13)$$

$$\delta_{\text{out}} = a'_\delta V_{\text{rate}-\delta} + b'_\delta \quad (14)$$

Here, $a_{\delta(j)}$ and $a_{\delta(j+1)}$ are the slope of the linear interpolation in the table and $b_{\delta(j)}$ and $b_{\delta(j+1)}$ are also the intercept. $d_{(j)}$ and $d_{(j+1)}$ are index distance of the table and j is the index number. In the tilt angle detection, first, we detected the distance output d_{out} using the distance mode and calculated the slope a'_δ and the intercept b'_δ. Then, we calculated the tilt output δ_{out} using the slope and the intercept.

Fig. 9 shows the tilt angle output at fixed distances. The horizontal axis of each graph is the tilt angle δ of the object surface, and the vertical axis is tilt output δ_{out}. As shown in the figure, the maximum error at the origin was $1.45°$. The error at the origin was made small by calibration, and the tilt detection accuracy at short distance was improved. At a distance of 2.8 mm, the error was $-0.85°$.
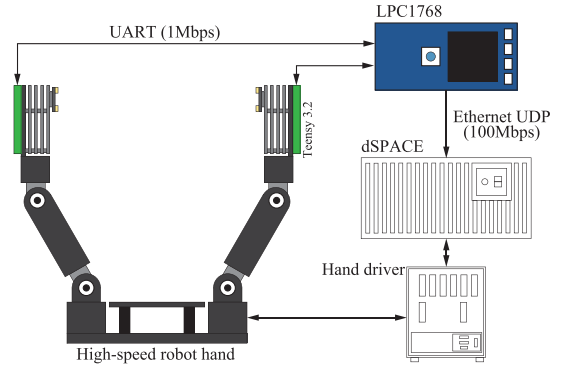

Fig. 10. Connection diagram of the hand system. The outputs of two sensors were processed by Teensy 3.2 and transmitted to LPC1768 via UART (1 Mbps). LPC1768 simultaneously received data from the two Teensy 3.2 and transmitted the distance value to the real-time controller (dSPACE) by Ethernet communication (UDP, 100 Mbps).

IV. GRASPING EXPERIMENT

We installed the sensors in a high-speed robot hand system and carried out an experiment to catch a paper balloon. Fig. 10 shows the connection diagram of the system. The fingers of the high-speed robot hand could open and close by 180 degrees in 0.1 seconds. Two proximity sensors were mounted on the two fingers of the hand. The outputs of the sensors were processed by Teensy 3.2 mounted on the back of the fingertip and were transmitted to the microcontroller (LPC1768) via UART (1 Mbps). LPC1768 simultaneously received UART data from the two sensors and transmitted the distance value to the real-time controller (dSPACE) via Ethernet communication (100 Mbps, UDP).

The total delay time of the UART and Ethernet communication was 61.1 μs. The total execution time was 829.1 μs since one measurement time was 768 μs. Therefore, we realized a measurement period of 1 ms order with this system.

The control program carried out position control and contact detection of each finger from the distance value detected by each fingertip. In order to calculate the target position of the fingertip, the target distance (the rubber thickness of the contact surface) was subtracted from the detected distance and the current fingertip position was added to this deviation. Finally, inverse kinematics were applied to the target position to obtain the target value of the joint angles, and the two flexion joints of each finger were controlled by angle-based PD control. Here, the posture of the fingertip was constant and only the distance was controlled.

We used two conditions for contact detection. First, the distance detected by the sensor was equal to or less than the target distance (thickness of rubber sheet on the contact surface). Second, there was a deviation between the change in the fingertip position calculated by forward kinematics and the distance change of the sensor. The first condition enables a contact detection for rigid objects. The second condition enables the detection for soft objects having an uneven surface. In the second condition, the amount of change of the fingertip position Δx and the distance change Δd are updated when the fingertip position changes by 0.1 mm. When the difference between the two val-
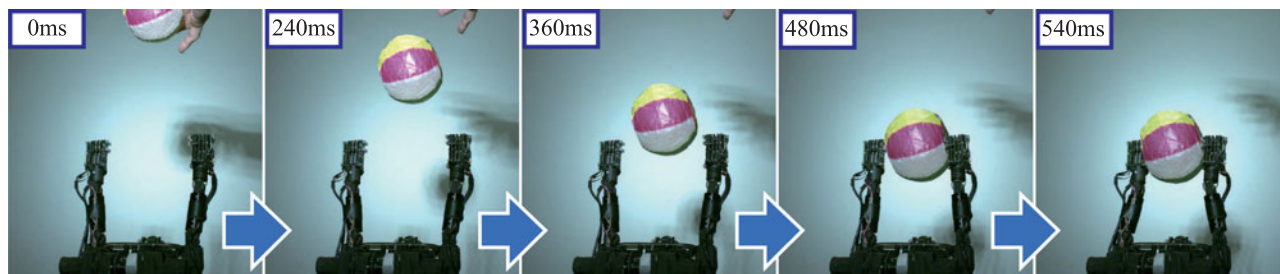
Fig. 11. Experimental result of catching a paper balloon dropped from a height of about 20 cm. At about 480 ms, the right finger was stopped as a result of contact detection, and the left finger was stopped at about 540 ms. The hand caught the balloon without crushing it.

ues $\Delta x - \Delta d$ reached 0.09 mm or more, the robot determined that contact occurred.

Fig. 11 is a series of continuous photographs captured when catching the paper balloon dropped from a height of about 20 cm. A paper balloon is a traditional Japanese toy and is formed into a spherical shape by alternately stitching different sheets of glassine paper. Since the thickness of the paper was 0.1 mm or less, its surface was very easily deformed. The hand was able to catch the paper balloon with a deformation equal to or less than that achievable by a human performing the same catching task. A video of the catching experiments is available at the following url:

https://www.youtube.com/watch?v=UVMg2qdhdYs

V. Conclusion

We developed a compact proximity sensor that detects the distance to and the tilt angle of the surface of an object with the peak-to-peak distance error less than 1/129-th ($< 31 \mu$m) and the measuring time less than 1/10-th (<1 ms) those of existing sensors. In addition, we installed these sensors on the fingertips of a high-speed robot hand and realized high-speed catching of a fragile object (paper balloon). We demonstrated robust contact detection for the paper balloon, having various surface colors and an uneven surface, with proximity sensing alone. High-speed grasping of the object with extremely small contact force was possible by feeding back the proximity sensor outputs.

In future work, we challenge to detect the distance to a specularly reflected object and improve the maximum detection distance of the sensor. We also realize force control based on accurate proximity sensor feedback.

References

[1] K. Koyama, H. Hasegawa, Y. Suzuki, A. Ming, and M. Shimojo, "Pre-shaping for various objects by the robot hand equipped with resistor network structure proximity sensors," in *Proc. IEEE/RSJ Int. Conf. Intell. Robots Syst.*, 2013, pp. 4027–4033.

[2] K. Koyama, Y. Suzuki, A. Ming, and M. Shimojo, "Integrated control of a multi-fingered hand and arm using proximity sensors on the fingertips," in *Proc. IEEE Int. Conf. Robot. Automat.*, 2016, pp. 4282–4288.

[3] H. Alagi, S. E. Navarro, M. Mende, and B. Hein, "A versatile and modular capacitive tactile proximity sensor," in *Proc. IEEE Haptics Symp.*, 2016, pp. 290–296.

[4] P. Radhen and C. Nikolaus, "Integrated force and distance sensing using elastomer-embedded commodity proximity sensors," *Robot., Sci. Syst.*, 2016, doi: 10.15607/RSS.2016.XII.035.

[5] K. Hsiao, P. Nangeroni, M. Huber, A. Saxena, and A. Y. Ng, "Reactive grasping using optical proximity sensors," in *Proc. IEEE Int. Conf. Robot. Automat.*, 2009, pp. 2098–2105.

[6] J. Konstantinova, A. Stilli, A. Faragasso, and K. Althoefer, "Fingertip proximity sensor with realtime visual-based calibration," in *Proc. IEEE/RSJ Int. Conf. Intell. Robots Syst.*, 2016, pp. 170–175.

[7] B. Yang, P. Lancaster, and J. R. Smith, "Pre-touch sensing for sequential manipulation," in *Proc. IEEE Int. Conf. Robot. Automat.*, 2017, pp. 5088–5095.

[8] X. Chen *et al.*, "Development of a low-cost ultra-tiny line laser range sensor," in *Proc. IEEE/RSJ Int. Conf. Intell. Robots Syst.*, 2016, pp. 111–116.

[9] K. Shimonomura, H. Nakashima, and K. Nozu, "Robotic grasp control with high-resolution combined tactile and proximity sensing," in *Proc. IEEE Int. Conf. Robot. Automat.*, 2016, pp. 138–143.

[10] H. K. Lee, S. I. Chang, and E. Yoon, "Dual-mode capacitive proximity sensor for robot application: Implementation of tactile and proximity sensing capability on a single polymer platform using shared electrodes," *IEEE Sens. J.*, vol. 9, no. 12, pp. 1748–1755, Dec. 2009.

[11] Y. S. Kim, S. I. Cho, D. H. Shin, J. Lee, and K. H. Baek, "Single chip dual plate capacitive proximity sensor with high noise immunity," *IEEE Sens. J.*, vol. 14, no. 2, pp. 309–310, Feb. 2014.

[12] S. Tsuji and T. Kohama, "Tactile and proximity sensor using self-capacitance measurement on curved surface," in *Proc. IEEE Int. Conf. Ind. Technol.*, 2017, pp. 934–937.

[13] X. Lü *et al.*, "A novel proximity sensor based on parallel plate capacitance," *IEEE Sens. J.*, 2017, doi: 10.1109/JSEN.2017.2787755.

[14] H. S. Han, J. Park, and T. D. Nguyen, "A highly sensitive dual mode tactile and proximity sensor using Carbon Microcoils for robotic applications," in *Proc. IEEE Int. Conf. Robot. Automat.*, 2016, pp. 97–102.

[15] R. Masuda, "Multifunctional optical proximity sensor using phase modulation," *J. Robotic Syst.*, vol. 3, no. 2, pp. 137–147, 1986, doi: 10.1002/rob.4620030203.

[16] L. Orozco, "Synchronous detectors facilitate precision, low-level measurements," *Analog Dialogue*, vol. 48, no. 11, pp. 1–5, 2014.

[17] C. Qi, Y. Huang, W. Zhang, D. Zhou, Y. Wang, and M. Zhu, "Design of dual-phase lock-in amplifier used for weak signal detection," in *Proc. Annu. Conf. IEEE Ind. Electron. Soc.*, 2016, pp. 883–888.

[18] X. Wang, S. Liu, and H. Shinoda, "Micro optical position sensor with vibrating light source," in *Proc. Tech. Dig. 17th Sens. Symp.*, 2000, pp. 137–140.